

## Supporting Information

### **Polyazomethines and their acid-base interactions with Nafion and Nafion-imidazole membranes for efficient fuel cells**

Marek Malinowski<sup>1,4\*</sup>, Agnieszka Iwan<sup>2\*\*</sup>, Igor Tazbir<sup>1</sup>, Bartosz Boharewicz<sup>1</sup>, Andrzej Sikora<sup>1</sup>,  
Andrzej Stafiniak<sup>3</sup>

<sup>1</sup>*Electrotechnical Institute, Division of Electrotechnology and Materials Science,  
M. Skłodowskiej-Curie 55/61, 50-369 Wrocław, Poland, \*e-mail: [malinowski.137@gmail.com](mailto:malinowski.137@gmail.com)  
phone: +48 71 328 30 61, fax: +48 71 328 25 51*

<sup>2</sup>*Military Institute of Engineer Technology, Obornicka 136 Str., 50-961 Wrocław, Poland, \*\*e-  
mail: [iwan@witi.wroc.pl](mailto:iwan@witi.wroc.pl)*

<sup>3</sup>*Faculty of Microsystem Electronics and Photonics, Wrocław University of Technology,  
Janiszewskiego str. 11/17, Wrocław, Poland*

<sup>4</sup>*Hydrogen South Africa (HySA) Systems and Validation Centre, SAIAMC, University of the  
Western Cape, Robert Sobukwe Road, Bellville, Cape Town, South Africa*

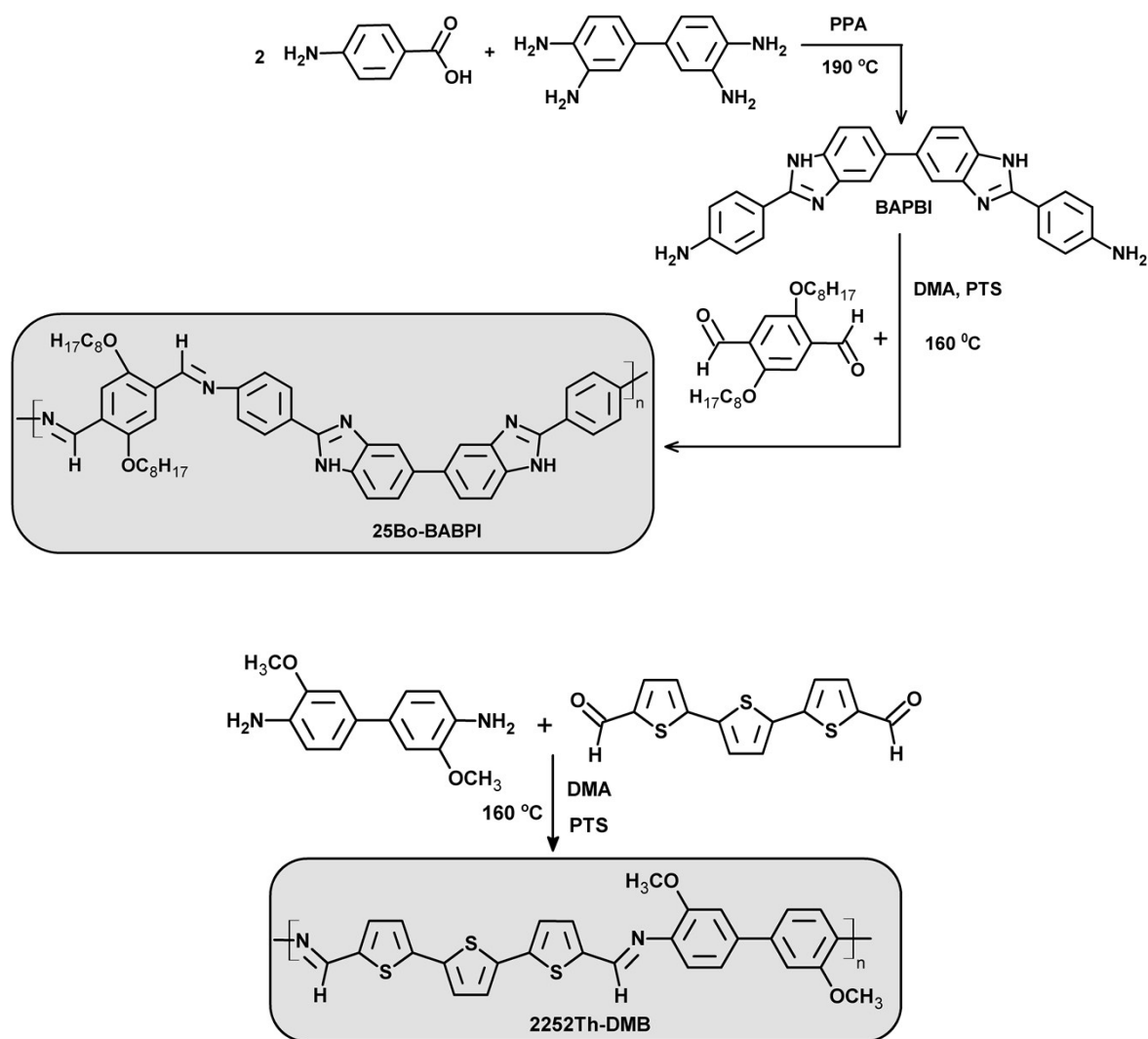


Fig. S11. Synthetic route of 25Bo-BABPI and 2252Th-DMB polyazomethines

### Synthesis of 25Bo-BABPI

The polymer was obtained applying a one-step high temperature condensation technique with anhydrous  $\text{CaSO}_4$  used as a water trap. A single-neck flask with a magnetic stir bar was charged with dialdehyde (1 mmol), BAPBI diamine (1 mmol), *p*-toluenesulfonic acid (PTS) and 10 mL of DMA. The reaction mixture was allowed to stir for 22 h at 160 °C in an oil bath. The polymer solution was precipitated in methanol, and the polymer was collected by filtration. The solid was washed with hot methanol and hot acetone. The final polymer was dried overnight at 80 °C. The Yield was ca. 60 %. FTIR (KBr pellet),  $\nu$  [ $\text{cm}^{-1}$ ]: 2924-2855 (aliphatic

C-H stretching), 1672 (C=O stretching from residue CHO groups), 1615 (C=N imine stretching), 1591-1457 (stretching in the aromatic ring), 1426 (C-H bending), 1199 (aromatic C-O stretching), 1018 (aliphatic C-O stretching).

#### *Chemical oxidation of polyazomethines*

Doping of 2252Th-DMB polymer with FeCl<sub>3</sub> was performed in chloroform (CHCl<sub>3</sub>) solution, while for 25Bo-BABPI DMA solvent was used. Due to the moisture sensitivity of FeCl<sub>3</sub>, the solution preparation were done in a glove-box filled with argon. The resulting absorbance spectra after the addition of the FeCl<sub>3</sub> were subsequently recorded. UV-Vis spectra in a chloroform and DMA solution were recorded on a Jasco V670 spectrophotometer.

#### Experimental

The surface morphology investigations of the membranes were performed in air using a commercial Innova AFM system from Bruker (former Veeco) company with implemented Dynamic Scanning Rate feature [1]. Topography imaging was performed using Tapping Mode with Phase Imaging feature. The NSG30 probes from NT-MDT ( $k = 22-100 \text{ N m}^{-1}$ ,  $f_{\text{res}} = 240-440 \text{ kHz}$ ,  $r_{\text{tip}} = 6 \text{ nm}$ ) were used. Force spectroscopy measurements were performed using CSG30 probes from NT-MDT ( $k = 0.13-2 \text{ N m}^{-1}$ ,  $f_{\text{res}} = 26-76 \text{ kHz}$ ,  $r_{\text{tip}} = 6 \text{ nm}$ ). The spring constant of the cantilever was determined using calibration feature from Nanoidea company [2,3]. The data was processed using SPIP software from Image Metrology [4].

Surface morphology and chemical composition were examined by Field Emission - Scanning Electron Microscope (FE-SEM, Hitachi SU6600) equipped with an adapter for Energy-Dispersive X-ray spectroscopy (EDX, Thermo Scientific NORAN System 7). SEM imaging was performed with the acceleration voltage of electron beam 15 kV and the samples 30 degrees tilt. Microanalysis of surface chemical composition was carried out using 15

keV electron beam energies. In order to averaging the measured values each samples were three times investigated at the area of  $635 \mu\text{m} \times 476 \mu\text{m}$ .

- [1] A. Sikora, Ł. Bednarz, Dynamic speed control in atomic force microscopy to improve imaging time and quality, Measurement Science and Technology, 2014, **25** 044005.
- [2] M. Ekwińska, Z. Rymuza, Normal Force Calibration Method Used for Calibration of Atomic Force Microscope. Acta Phys. Pol., 2009, **116** 78–81.
- [3] A. Sikora, L. Bednarz, G. Ekwiński, M. Ekwińska, The determination of the spring constant of T-shaped cantilevers using calibration structures, Measurement Science and Technology, 2014, **25** 044015.
- [4] <http://www.imagemet.com/> accessed 25.09.2014

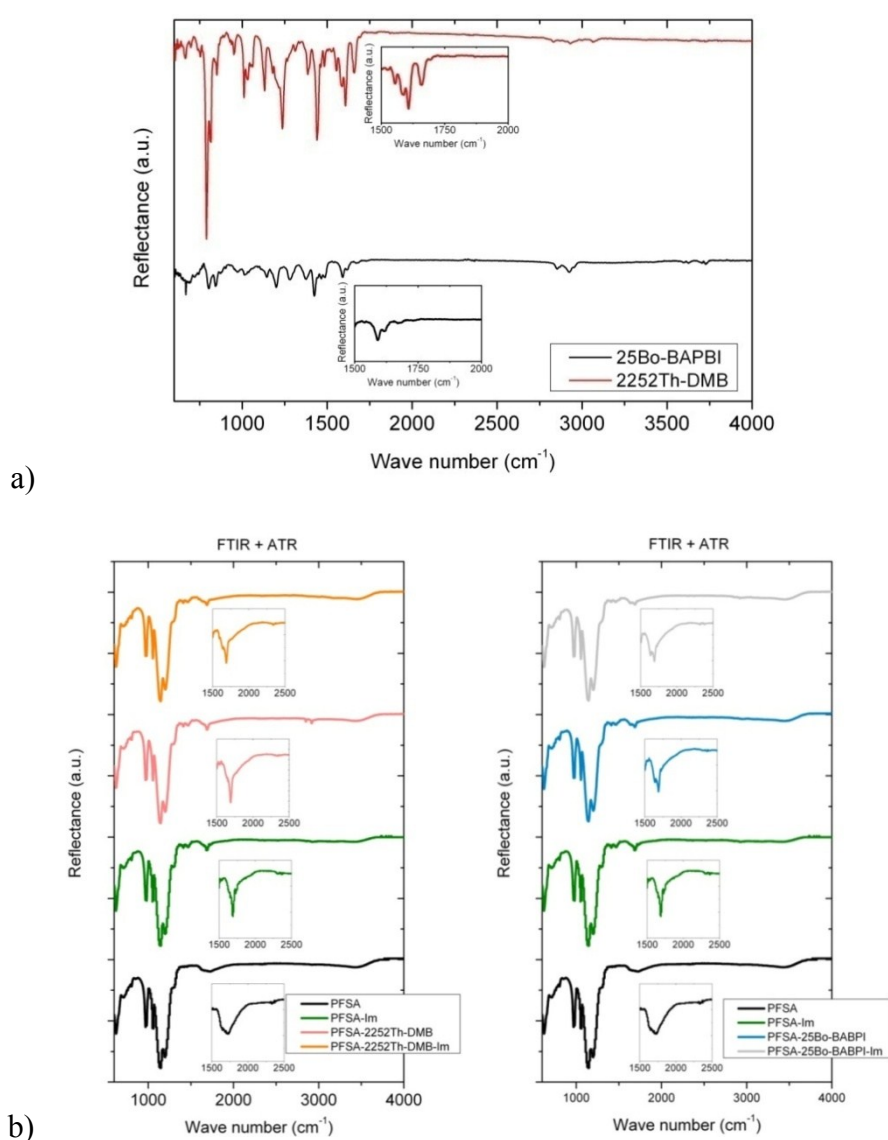


**Fig. SI2a.** FTIR spectra of (a) 25Bo-BABPI and 2252Th-DMB and (b) pristine PFSA, binary, and ternary membranes

## TGA and DTG analyses

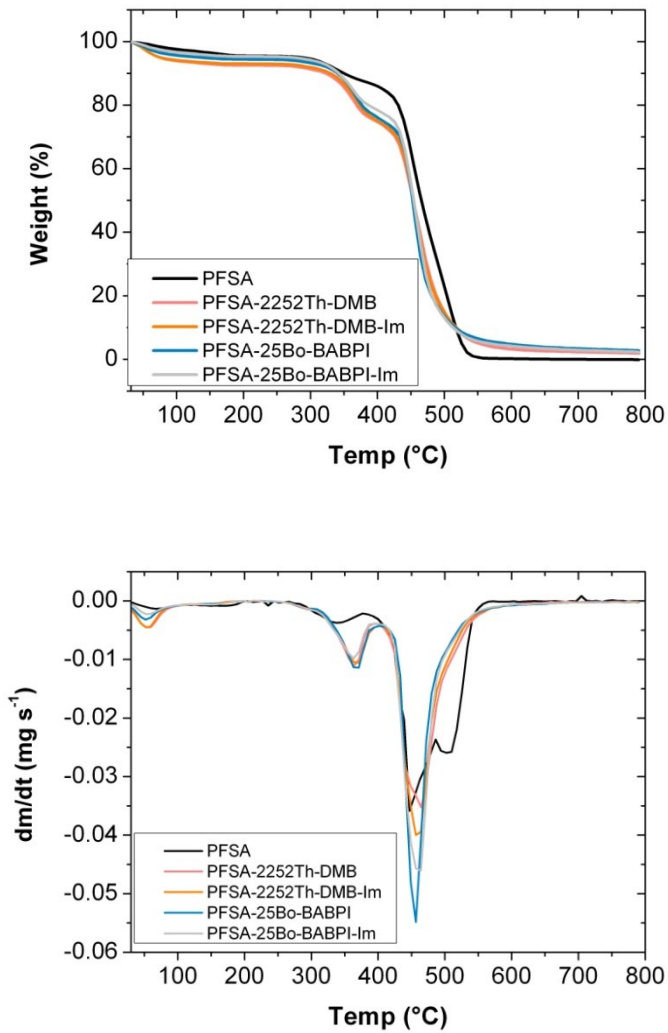
In Table SI1 numerical data are collected depicting temperature of 10 and 20% weight loss for particular membranes and temperature at which maximum rate of weight loss was detected.

Table SI1. Thermal stability of investigated membranes by TGA method

Code	T <sub>10%</sub> [°C] <sup>a</sup>	T <sub>20%</sub> [°C] <sup>a</sup>	T <sub>p</sub> [°C] <sup>b</sup>	T <sub>p</sub> [°C] <sup>b</sup>
PFSA	350	431	338	447, 502
PFSA-Im	357	398	369	455
PFSA-2252Th-DMB	322	369	366	454
PFSA-2252Th-DMB-Im	330	373	370	459
PFSA-25Bo-BABPI	340	376	370	455
PFSA-25Bo-BABPI-Im	343	387	369	456

<sup>a</sup>T<sub>5%</sub>, T<sub>10%</sub>, T<sub>25%</sub>: temperatures at 10, 20% weight loss, <sup>b</sup>temperatures at which the maximum rate of weight loss was observed according to DTG curves

TGA analysis of pristine PFSA membrane revealed three peaks at 338, 447 and 502 °C according DTG graphs. This material started to decompose at temperature above 300 °C i.e. it lost 10% of weight at 350 °C and 20% at 431 °C that clearly demonstrates its thermal stability and therefore suitability to be applied as fuel cell electrolyte. Both polyazomethine, 2252Th-DMB with thiophene rings and 25Bo-BABPI with bibenzimidazole groups as well as imidazole have various influence on PFSA membrane thermal stability. Imidazole slightly improved thermal properties of PFSA membrane, for which 10% of weight loss was at 357 °C, however both polyazomethines had negative impact on thermal properties but this deterioration was relatively small. It was measured that 10% of weight loss occurred at 322 and 340 °C for PFSA-2252Th-DMB and PFSA-25Bo-BABPI, and 330 and 343 °C for PFSA modified with 2252Th-DMB-Im and 25Bo-BABPI-Im, respectively (see Fig. SI3).



**Fig. SI3.** TGA and DTG thermographs of PFSA membranes obtained in nitrogen atmosphere

### Water uptake

H<sub>2</sub>O molecules are the main charge carriers in the electrolyte structure, therefore the amount of water inside the membrane determines the value of ionic conductivity and fuel cell performance. The water uptake (WU) was calculated from the equation

$$WU = \frac{m_w - m_d}{m_d} \cdot 100\%$$

, where  $m_w$  is a weight of wet membrane, and  $m_d$  the weight of dry membrane.

The value of water uptake describes the polymer swelling and fixed charge concentration. However, high dependency of membrane conductivity on water uptake is a

disadvantage. Therefore, in this paper the water uptake was calculated for selected composite membranes to determine this dependency.

In order to calculate the water uptake, vapor sorption analysis was performed. For this purpose surface area and porosity analyzer was used to plot water sorption isotherms. Prior to measurement, all membranes were outgassed under high vacuum for 40 hours at 120 °C to ensure the water molecules were completely removed. The isotherms were plotted from the very low pressure (first point at 0.031 Pa) to the relative pressure of 0.9  $p/p^0$ , where  $p^0$  is the vapor saturation pressure.

### AFM and SEM study

The structure of the composite membranes was analyzed by AFM technique using both: topography and the phase imaging data, which reveals the viscous-elastic properties of the surface, very often correlated with the structure of investigated material. Such parameters as roughness ( $R_a$ ,  $R_{ms}$ ), skewness (the unbalance of height distribution maximum) and kurtosis (the peak's width on height distribution) were calculated. Mentioned parameters are presented in Table SI2. The analysis of the topography image of PFSA sample at submicron scale reveals the presence of elongated, highly oriented grains of size approx. 10/40 nm. The calculated  $S_{tdi}$  factor (Texture Direction Index) is 0.45, which indicates the surface anisotropy. Large scale area scans (10  $\mu\text{m} \times 10 \mu\text{m}$ ) show the presence of crater-like features of diameter 5  $\mu\text{m}$  covering a significant fraction of the surface.

Table SI2. The surface parameters of all membranes investigated by AFM

Code	Surface statistics*				
	$R_a$ [nm]	$R_{ms}$ [nm]	Skew	Kurtosis	Surface Area Ratio [%]
<b>PFSA</b>	1.2021	1.5789	0.1858	4.8332	6.537
<b>PFSA-Im</b>	0.3279	0.4502	0.5294	7.2920	2.787
<b>PFSA-2252Th-DMB</b>	0.3524	0.4828	1.2228	7.0364	2.287
<b>PFSA-25Bo-BABPI</b>	3.1760	3.9659	0.4129	2.7481	11.86
<b>PFSA-2252Th-DMB-Im</b>	0.8586	1.1176	-0.1458	5.4656	15.19
<b>PFSA-25Bo-BABPI-Im</b>	9.0361	11.159	0.1586	2.8475	21.88

\* values calculated for scanning field 300 nm  $\times$  300 nm ,  
 $R_a$ : value of the height irregularities (arithmetic average of absolute values). Exponent

(power) within the data variance sum for the RMS is  $q = 1$ . The Roughness Average, is defined as:  $R_a = \frac{1}{MN} \sum_{k=0}^{M-1} \sum_{l=0}^{N-1} |z(x_k, y_l)|$

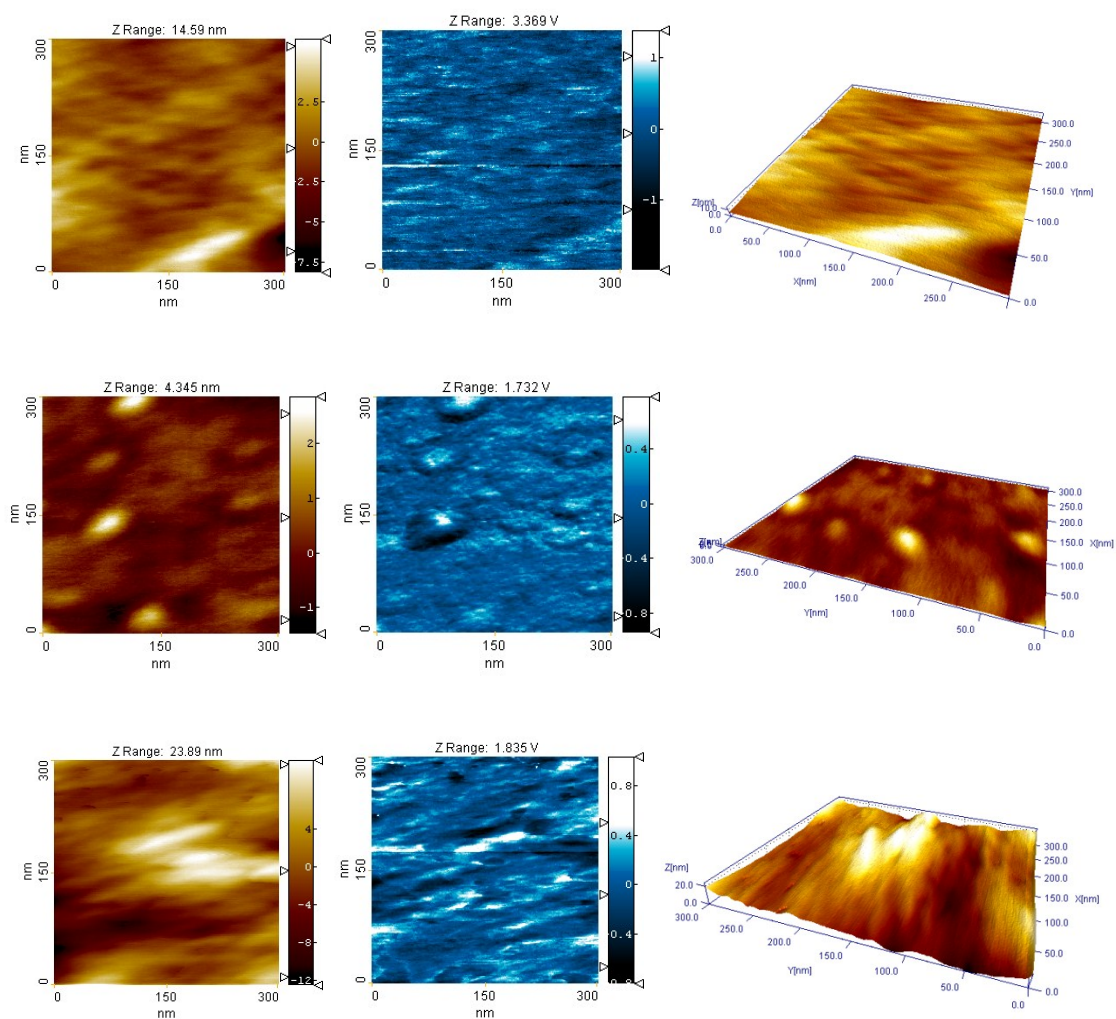
$R_{ms}$ : value of the height irregularities (Root Mean Squared). Exponent (power) within the data variance sum for the RMS is  $q=2$ . The Root Mean Square (RMS) parameter  $R_{ms} (S_q)$ , is defined as:  $R_{ms} = \sqrt{\frac{1}{MN} \sum_{k=0}^{M-1} \sum_{l=0}^{N-1} [z(x_k, y_l)]^2}$ , where: M and N are the total number of pixels in the analyzed scan, k and l are coordinates of a given pixel, z (x<sub>k</sub>, y<sub>l</sub>) is the height of the surface at a given coordinate.

The analysis of the morphology of the PFSA-2252Th-DMB sample allows noticing the presence of the raised oval features of the size in range from 50 nm to 300 nm. Some anisotropy of the surface can be also found: the orientation of the abovementioned features is coherent, as well as their formations in rows are visible (large area scans not shown here). This observation is confirmed by  $S_{tdi}$  factor reaching the value 0.65. 2D FFT analysis of the phase imaging data as well as direct analysis of the image, allowed defining the size of the grains about 6.6-6.7 nm. The analysis of both: topography and phase imaging data of the PFSA-25Bo-BABPI sample allows to notice a complex and developed structure of the surface. Large (150 nm long and 25 nm wide) grains can be distinguished. High anisotropy ( $S_{tdi} = 0.361$ ) can be also concluded. A substantial contrast of phase imaging between single grains is present, indicating large differences in viscous-elastic properties. Large area scans show the presence of groups of the grains creating hills-like features 300-400 nm in diameter.

In case of PFSA-Im sample, the surface is uniform. The typical sizes of grains are in the range of 60 nm in length and 20 nm in width. No significant phase imaging contrast is visible, showing rather the homogenous mechanical properties of the surface. Large area scans show a significant anisotropy of the surface.  $S_{tdi}$  value reaches 0.32. Moreover, the presence of the micrometers scale features revealing some linear structure can be also distinguished. The analysis of the topography image of the PFSA-2252Th-DMB-Im sample allowed noticing the presence of the high density of pores of 20-40 nm in diameter. The size of the grains can be estimated to be approx. 5 nm. A slight orientation of the structures is visible –  $S_{tdi} = 0.536$ . The

phase imaging shows relatively mechanically-homogenous surface. Large areas scans show the presence of 500-1000 nm hill-like features.

The analysis of the surface of the PFSA-25Bo-BABPI-Im sample shows a large roughness, and high orientation of the grains and large size features (of few micrometers in size when measured as the groups).  $S_{tdi} = 0.237$  The phase imaging reveals the significant contrast allowing to determine the size of the grains to be approx. 15 nm. Fig. SI5 shows AFM images obtained for all created membranes.



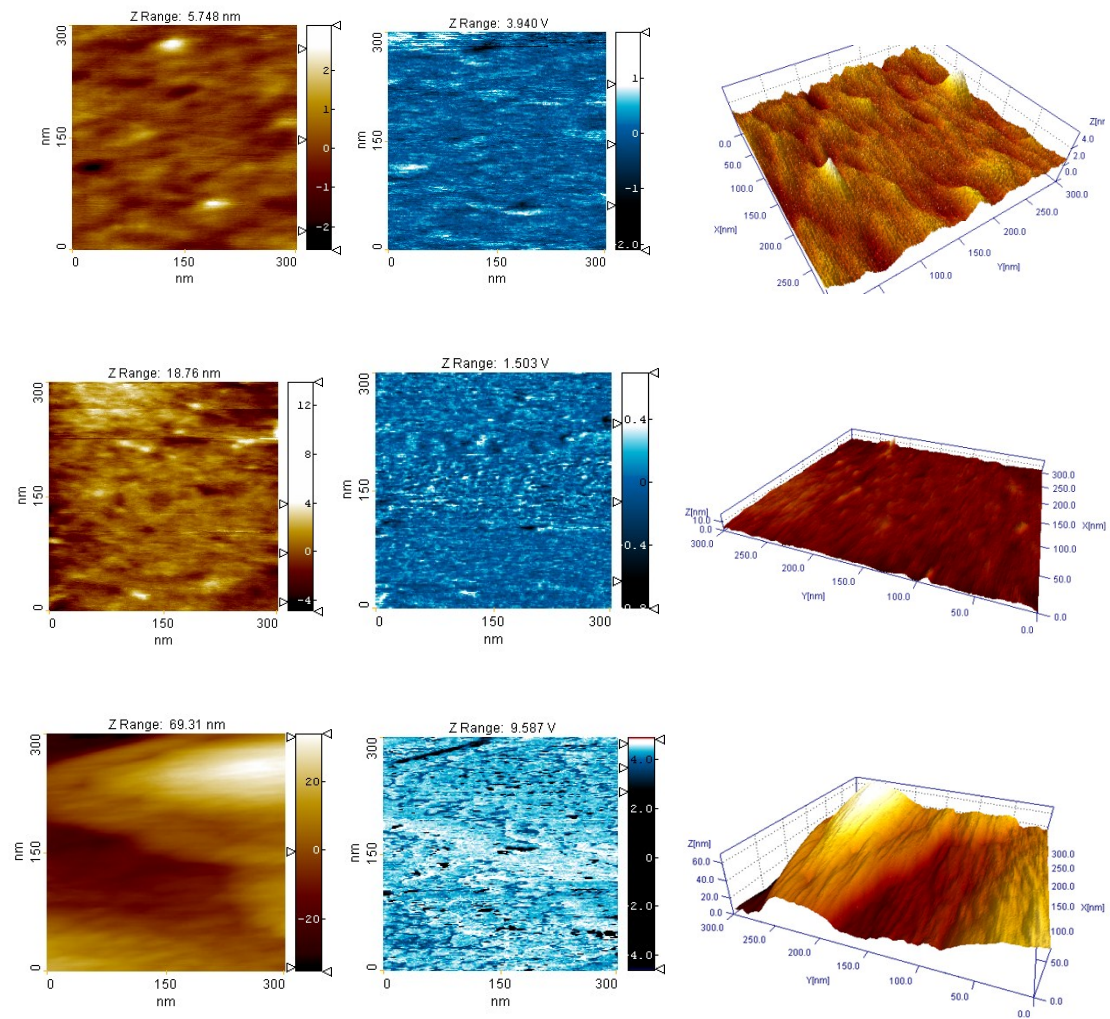
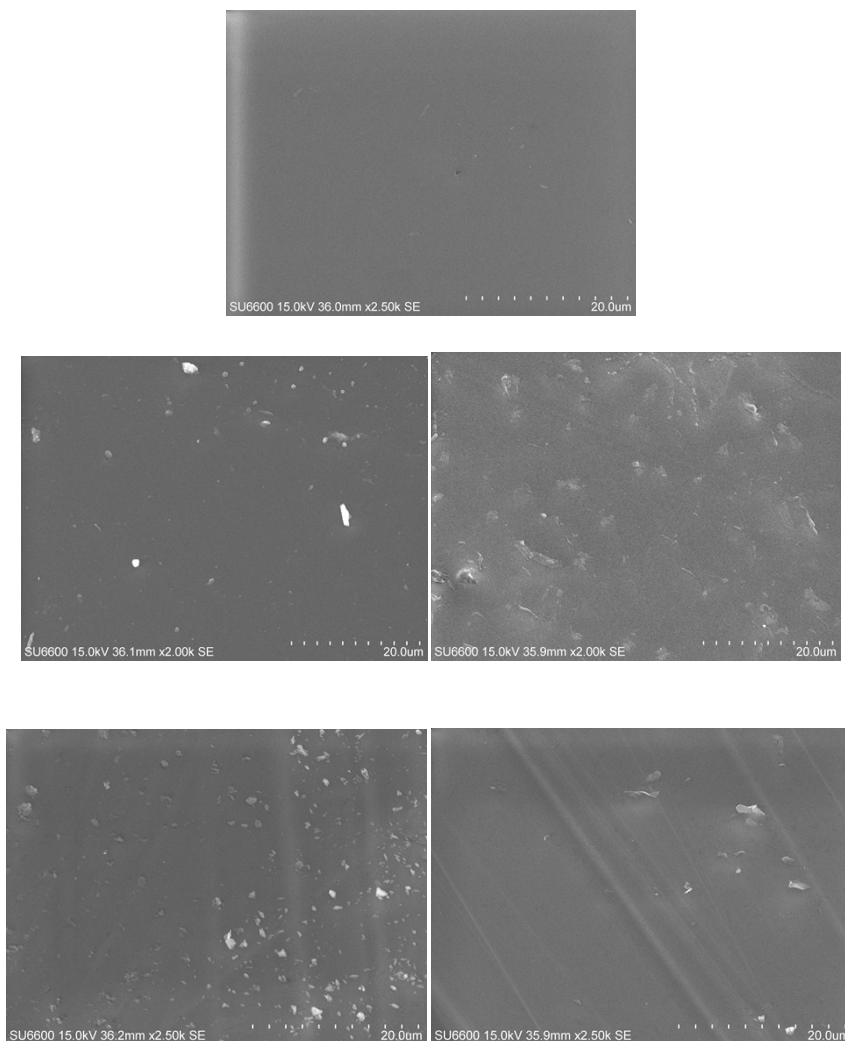


Fig. SI5. Topography, phase imaging, and 3D view of the topography measured with AFM for PFSA, PFSA-2252Th-DMB, PFSA-25Bo-BABPI, PFSA-Im, PFSA-2252Th-DMB-Im and PFSA-25Bo-BABPI-Im, from top to bottom respectively.

Additionally, the morphology of the modified membranes was investigated by SEM (see Fig. SI6).



**Fig. SI6.** SEM images of PFSA, PFSA-25Bo-BABPI, PFSA-25Bo-BABPI-Im, PFSA-2252Th-DMB, PFSA-2252Th-DMB-Im and from top to bottom, from left to right, respectively.

The presence of polyazomethines/imidazole in PFSA membranes was also confirmed by EDX analysis with assumption that there are no nitrogen atoms in pristine membranes according to the chemical structure of PFSA. It was found that nitrogen atoms are present in the spectra of PFSA-25Bo-BABPI, PFSA-25Bo-BABPI-Im, PFSA-2252Th-DMB and PFSA-2252Th-DMB-Im in the amount of 5.04, 5.48, 4.95, and 5.04 % of atomic weight, respectively. The membranes showed a uniformity of chemical composition regardless of the measured area. In Fig. SI7 the EDX elemental mapping of the surface of PFSA-2252Th-DMB-Im is presented, as an example.

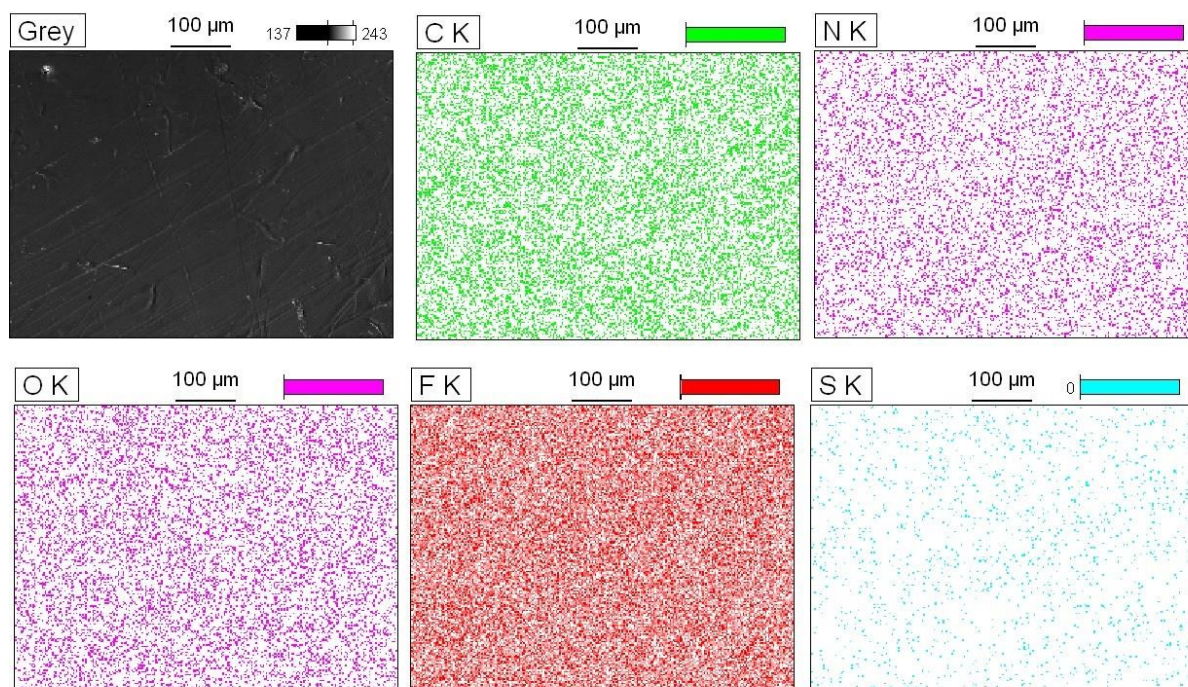


**Fig. SI7.** EDX elemental mapping of the surface of PFSA-2252Th-DMB-Im

### **Chemical oxidation of polyazomethines**

In most cases polyazomethines are hydrolytically and anodically unstable, however it is general conclusion. The chemical oxidation properties of polyazomethines strongly depend on the chemical structure of the investigated compounds [5, 6]. In order to analyze their chemical stability, the chemical doping of 2252Th-DMB polymer with  $\text{FeCl}_3$  was done in chloroform ( $\text{CHCl}_3$ ) solution whereas for 25Bo-BABPI doped with  $\text{FeCl}_3$  dimethylacetamide was used as solvent. The absorbance changes upon oxidizing of both polyazomethines with iron (III) chloride are presented in Fig. SI8.

In a chloroform solution, 2252Th-DMB doped with  $\text{FeCl}_3$  exhibited very small hypsochromic shift of the absorption band maximum (responsible for the  $\pi-\pi^*$  transition in the imine group) in comparison with the maximum of undoped 2252Th-DMB (i.e. from 415 nm to 410 nm).

Similar behaviour was found for 25Bo-BAPBI doped with  $\text{FeCl}_3$  (see Fig. SI8). The addition of  $\text{FeCl}_3$  to polyazomethines resulted in the increase of absorption intensity compared with undoped one. The absence of significant change in the absorbance spectra between the undoped and doped polyazomethines confirms the oxidative stability of the investigated polyazomethines. As it is known [6] the large hypsochromic shift decrease in intensity and even total decrease of the absorbance would be observed if the polymers decomposed or hydrolyzed during oxidation.

[5] S. Barik, S. Bishop, W.G. Skene, Spectroelectrochemical and Electrochemical Investigation of a Highly Conjugated All-Thiophene Polyazomethine. *Mat. Chem. Phys.* 129 (2011) 529-533.

[6] S. Barik, T. Bletzacker, W.G. Skene,  $\pi$ -Conjugated Fluorescent Azomethine Copolymers: Opto-Electronic, Halochromic, and Doping Properties. *Macromolecules* 45 (2012) 1165-1173.

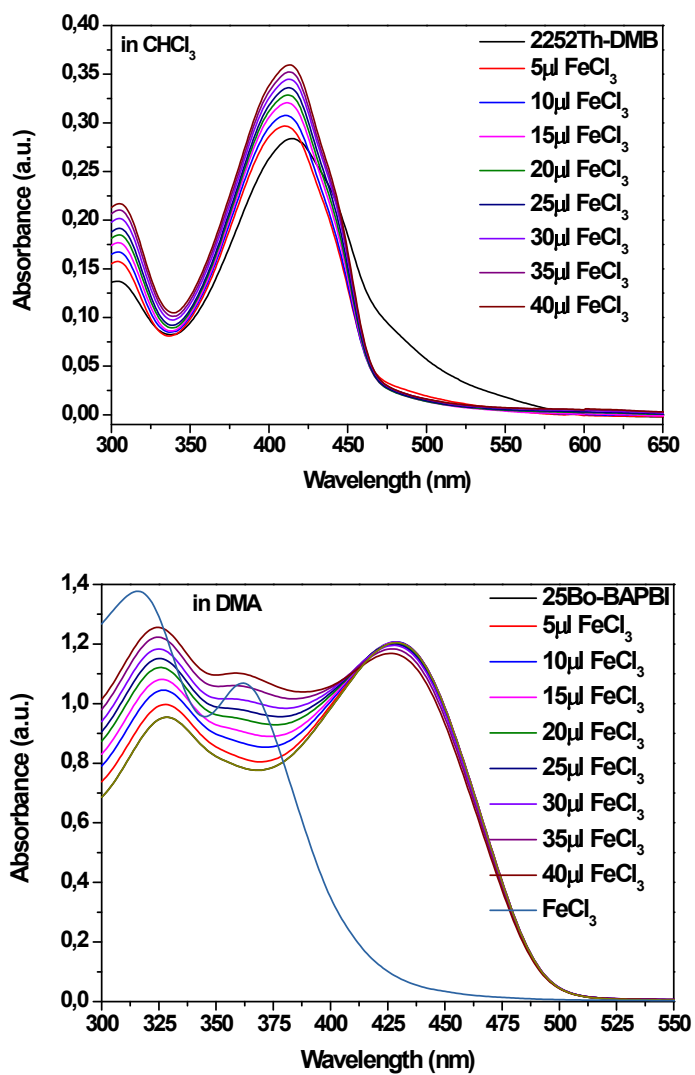


**Fig. S18.** Normalized absorbance spectra of both polyazomethines doped with FeCl<sub>3</sub>

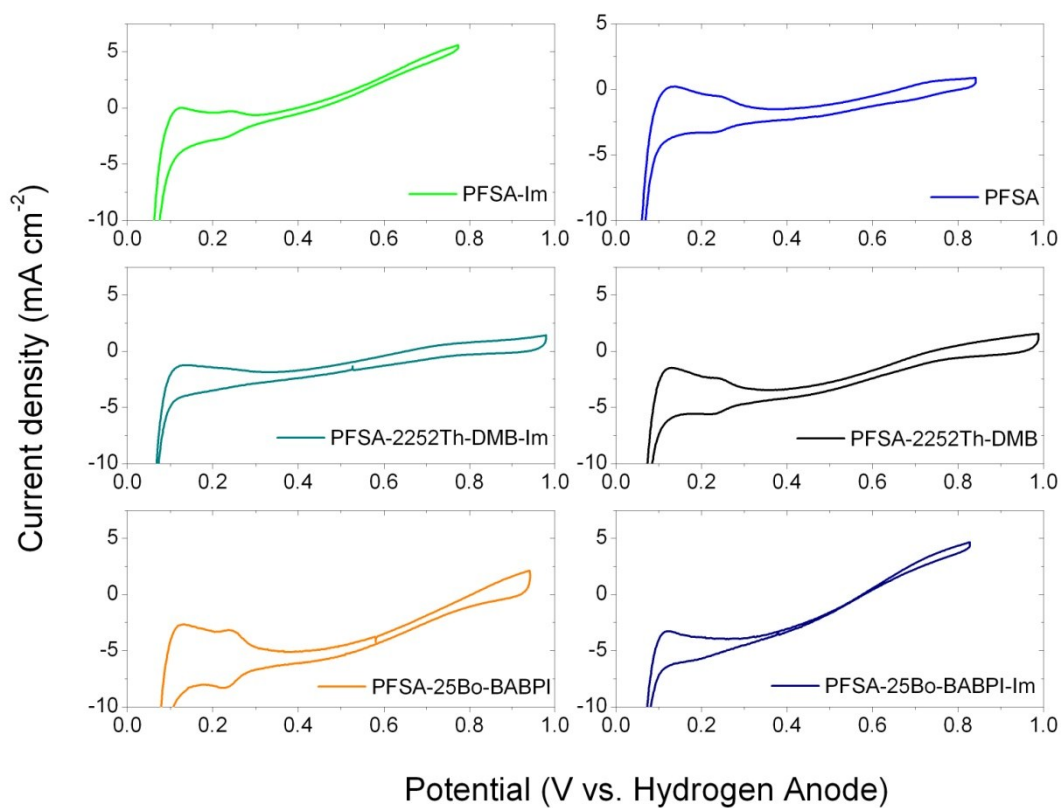


**Fig. SI9.** Cyclic voltammograms of particular polyazomethine and reference MEAs, performed at 25 °C, Rh90%, H<sub>2</sub>/Ar, 50/50 ml min<sup>-1</sup>

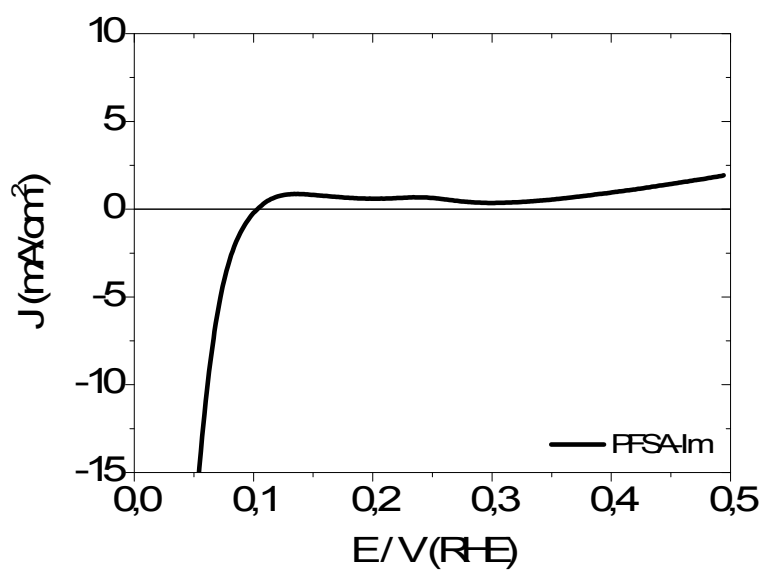


**Fig. SI10.** Linear Sweep Voltammetry of imidazole-modified PEMFC

The parameters such as exchange current density and Tafel slope were taken from IR-corrected polarization graphs extrapolating the curve to the lowest current density region. For the extrapolation, the Tafel equation was used:

$$\Delta V_{act} = a + b \log(i)$$

where  $\Delta V_{act}$  is activation losses,  $i$  – current density,  $b$  – Tafel slope and

$$a = -2.3 \frac{RT}{\alpha F} \log(i_0)$$

$$b = 2.3 \frac{RT}{\alpha F}, \text{ and}$$

$R$  – gas constant,  $T$  – temperature,  $\alpha$  – cathode transfer coefficient,  $F$  – Faraday's constant,  $i_0$  – exchange current density.

By plotting of IR-corrected overpotential-current relationship in a logarithmic scale (as shown below)  $b$ ,  $i_0$  and  $\alpha$  parameters were detected.

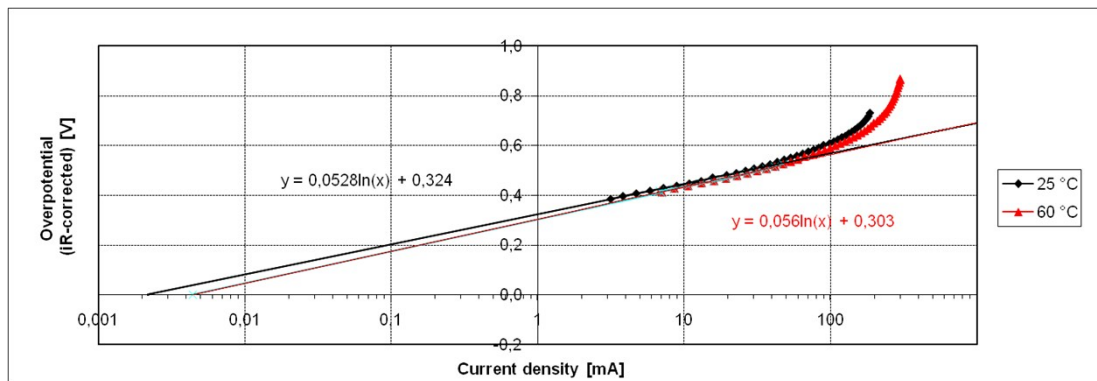


Fig. SI11. Potential losses versus current density (logarithmic scale) of PFSA due to activation and concentration polarizations

Applying these parameters, activation polarization losses were calculated at given current density (50 mA). Ohmic losses ( $iR$ ) were found taking the results of EIS measurements i.e. ionic conductivity of electrolytes obtained from high frequency region of Nyquist plots. Concentration polarization losses ( $\Delta V_{conc}$ ) were obtained from the equation:

$$\Delta V_{conc} = \left(1 + \frac{1}{\alpha}\right) \frac{RT}{nF} \ln\left(\frac{i_L}{i_L - i}\right)$$

where the limiting current density ( $i_L$ ) was calculated from the fitting of polarization curve in the region of concentration polarization:

$$f(x) = A \cdot \exp\left(\frac{-x}{t}\right) + y$$